Available online at www.sciencedirect.com
ScienceDirect
Journal of the European Ceramic Society 27 (2007) 3127–3133
www.elsevier.com/locate/jeurceramsoc

Uniaxial viscosity of gadolinium-doped ceria determined by discontinuous sinter forging

Jaemyung Chang [a], Olivier Guillon [b,*], Jürgen Rödel [b], Suk-Joong L. Kang [a]

[a] *Department of Materials Science and Engineering, Korea Advanced Institute of Science and Technology, 373-1 Guseong-dong, Yuseong-gu Daejeon 305-701, Republic of Korea*
[b] *Institute of Materials Science, University of Technology, Darmstadt D-64287, Germany*

Received 25 June 2006; received in revised form 21 December 2006; accepted 7 January 2007
Available online 15 February 2007

Abstract

The sintering behaviour of nanocrystalline gadolinium-doped ceria was investigated. The uniaxial viscosity determined from isothermal discontinuous sinter forging experiments. It increased dramatically during sintering from a few GPa·s at 85% to ~120 GPa·s at 97% relative density. These values, however, are much lower than those measured for other oxide materials with submicron sizes because of much finer grain size. Since the experiments were done under isothermal conditions, it is possible to evaluate separately the effects of the relative density and the grain size. Due to grain coarsening, the effect of grain size becomes significant at high relative density, as some available models predict. It was found that Rahaman's model best fit the experimental data.

Keywords: Sintering; Viscous behaviour; CeO_2; Fuel cells

1. Introduction

Intermediate temperature solid oxide fuel cells (IT-SOFCs) for temperatures below 700 °C are considered as alternative energy technology to the conventional systems because of high efficiency and reduced environmental pollution.[1,2] Among the candidates for the solid electrolyte of IT-SOFC, doped ceria systems have been considered to be the most promising due to their high electrical conductivity in an intermediate temperature range.[3,4]

Planar anode supported SOFC is a widely chosen geometry, because of its high power density and low fabrication cost. In order to reduce the fabrication costs, co-firing of anode/solid electrolyte is a promising technology.[5] Due to the difference of densification rates of components, sintering defects, such as cracks, debonding and warpage may occur. They act as obstacles for producing large area stacks.[1] Attempts for the co-firing process of SOFC components are evaluated from the sintering of a bilayer.[6] However, there have been few continuum mechanical approaches for understanding the co-firing processes of SOFC components yet.

Theoretical expressions of constitutive laws for sintering bodies[7–17] have been extensively studied, whereas experimental determination of the relevant parameters raised scientific interest in the last years.[18–25] By characterizing properties, such as bulk and shear viscosities (K_p and G_p, respectively) or uniaxial viscosity E_p and viscous Poisson's ratio ν_p, the sintering behaviour of bilayer components used in SOFC can be predicted.[26–28] In order to determine the viscosities, optical dilatometry,[20] cyclic loading[19,20] as well as discontinuous sinter forging[23–25] studies have been carried out. Using the viscoelastic analogy for the isotropic sintering bodies, the uniaxial viscosity can be determined from the free and axial strain rates ($\dot{\varepsilon}_f$ and $\dot{\varepsilon}_z$, respectively) measured along the direction of the applied stress σ_z:

$$E_p = \frac{\sigma_z}{\dot{\varepsilon}_z - \dot{\varepsilon}_f} \tag{1}$$

For the experimental evaluation of E_p, the microstructure should remain isotropic under the application of a load. Recently, Zuo et al.[23] reported a methodology to measure the sintering parameters using a discontinuous sinter forging procedure. They showed that the isotropic microstructure is maintained for alumina in a

* Corresponding author. Tel.: +49 6151 166362; fax: +49 6151 166314.
E-mail address: guillon@ceramics.tu-darmstadt.de (O. Guillon).

0955-2219/$ – see front matter © 2007 Elsevier Ltd. All rights reserved.
doi:10.1016/j.jeurceramsoc.2007.01.003

5% density range after load application provided that the stress remains under a threshold value.

In this study, we investigate the sintering behaviour of nanocrystalline doped ceria with a high resolution laser-assisted sinter forging apparatus and measure the uniaxial viscosity as a function of density at 1100 °C. Experimental data are compared to available models using a normalization both to viscosity at fixed density as well as to grain size. The results obtained can be employed to predict the sintering behaviour of multi-layered SOFC components.

2. Experimental procedure

Nanocrystalline gadolinium-doped ceria ($Ce_{0.9}Gd_{0.1}O_{2-\delta}$, denoted as GDC, Rhodia, Frankfurt, Germany) was used in this study. The mean diameter of GDC particles was determined by the BET method (Autosorb 3B, Quantachrome) was 24 m^2/g which is equivalent to 35 nm in average size under the assumption of spherical particles. Using a 12 mm diameter stainless steel mould, cylindrical samples were uniaxially dry-pressed at a pressure of 100 MPa. After cold isostatic pressing (at 350 MPa for 2 min), the green body density was measured from the dimension and found to be 60.7 ± 0.3% of the theoretical value.

The cylindrical pellets of 16 mm height were employed in sinter forging experiments using high-resolution axial and radial lasers[25] (precision ± 2 μm). Some pellets were freely sintered without external load whereas others were sintered freely up to a desired density at 1100 °C and then subjected to a constant load of either 50 or 100 ± 0.5 N, corresponding to 0.6 and 1.2 MPa, respectively. This mechanical loading was applied within a 5% increase of relative density. Heating and cooling rate was set to 30 °C/min. The density of each sintered specimen was determined by the Archimedes method. The microstructure was characterized on fracture surfaces. Grain size was measured by the linear intercept method with a correction coefficient of 1.56 using LINCE software (ver 2.31, Ceramics Group, TU Darmstadt). According to previous reports,[26,29] the mean grain size obtained from fracture surfaces is smaller than that measured on cross sections by 7%. A correction was made in this study. More than 250 grains were examined for each sample.

3. Results and discussion

The free densification behaviour at 1100 °C of GDC is shown in Fig. 1. Density can be determined at any time with the following relationship:

$$\rho = \frac{\rho_0}{\exp(\varepsilon_z + 2\varepsilon_r)} \quad (2)$$

where ρ_0 is the initial density and ε_z and ε_r are the true strains. At isothermal sintering, the initial relative density was 83.7% and the final relative density after 2 h sintering was 97.3%. Such high sintered densities had also been achieved in previous investigation using GDC nanopowders.[30,31] According to Kleinlogel and Gauckler,[30] the sintered GDC does not contain any liquid phase at 1200 °C, if samples are heated at a constant heating rate of 10 °C/min.

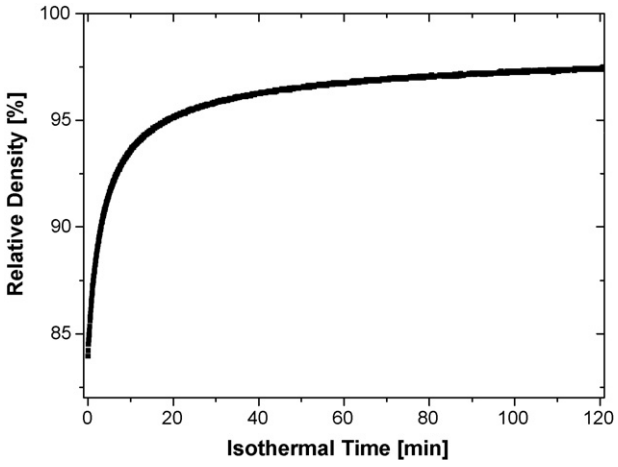

Fig. 1. Density of freely sintered samples as a function of isothermal time at 1100 °C.

The axial and radial strains at two different values of applied load as a function of isothermal time are shown in Fig. 2. Without external load, the shrinkage is isotropic. However, as the load increases, axial strain increases and radial strain decreases in an order of the external stress magnitude.

Discontinuous sinter forging provided a good linearity of the axial strain rate with respect to the applied load, as shown in

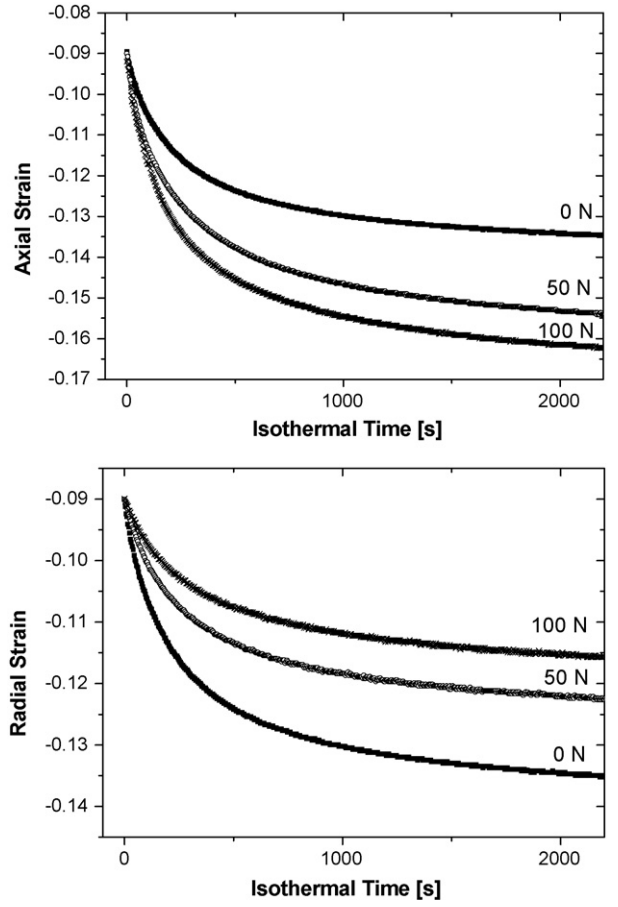

Fig. 2. (a) Axial and (b) radial strain as a function of sintering time. Sinter forging experiments were conducted by applying a uniaxial load of 50 and 100 N.

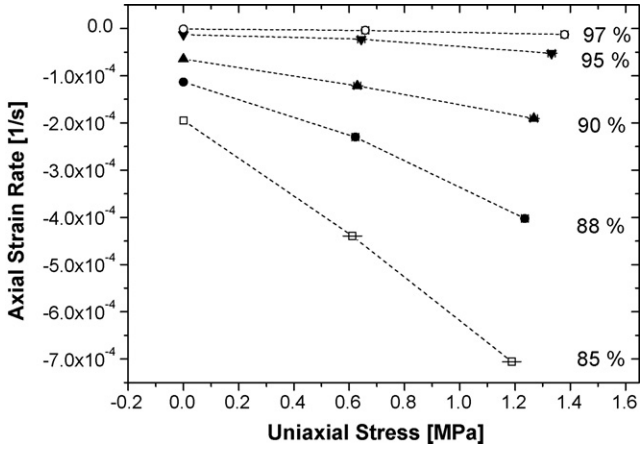

Fig. 3. Dependence of axial strain rate on applied stress at 1100 °C.

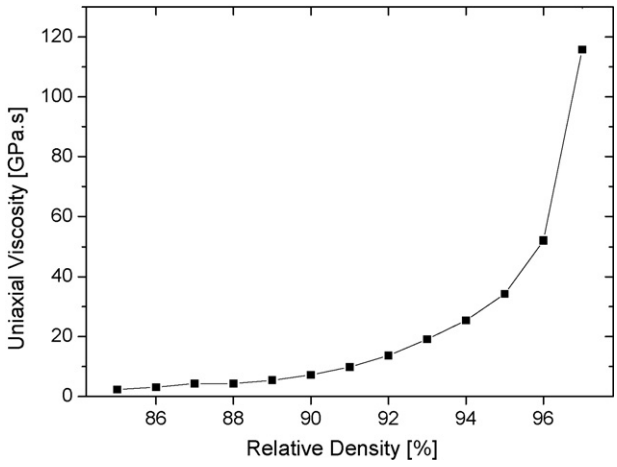

Fig. 4. Uniaxial viscosity as function of density at 1100 °C.

Fig. 3. This indicates that in the stress range considered, the material behaves viscoelastically and that the viscosity depends only on density and not on stress level. From Eq. (1), the slope of the linear plots for a given density corresponds to the inverse of the uniaxial viscosity. As density increases, viscosity increases, the free strain rate decreases, and the effect of the load is reduced. Fig. 4 shows the measured uniaxial viscosity E_p as a function of the relative density. As the relative density increases from 85 to ~ 90%, the viscosity increases quasi-linearly but remains low, less than 10 GPa s. However, it increases rapidly far further increase in relative density and becomes 118 GPa s at 97% relative density. The measured viscosities are very low compared with those of pure alumina samples at 1250 °C with an initial grain size of 150 nm (over 2500 GPa s).[24]

The big difference in measured viscosity between the GDC in the present investigation and the alumina in the previous investigation may be related to a difference in microstructural evolution. In a crystalline material, the uniaxial viscosity at a given temperature can be expressed in a general form[11,14,15,32,33]:

$$E_p = E_p^0 \times E_p^1(\rho) \times E_p^2(d) \tag{3}$$

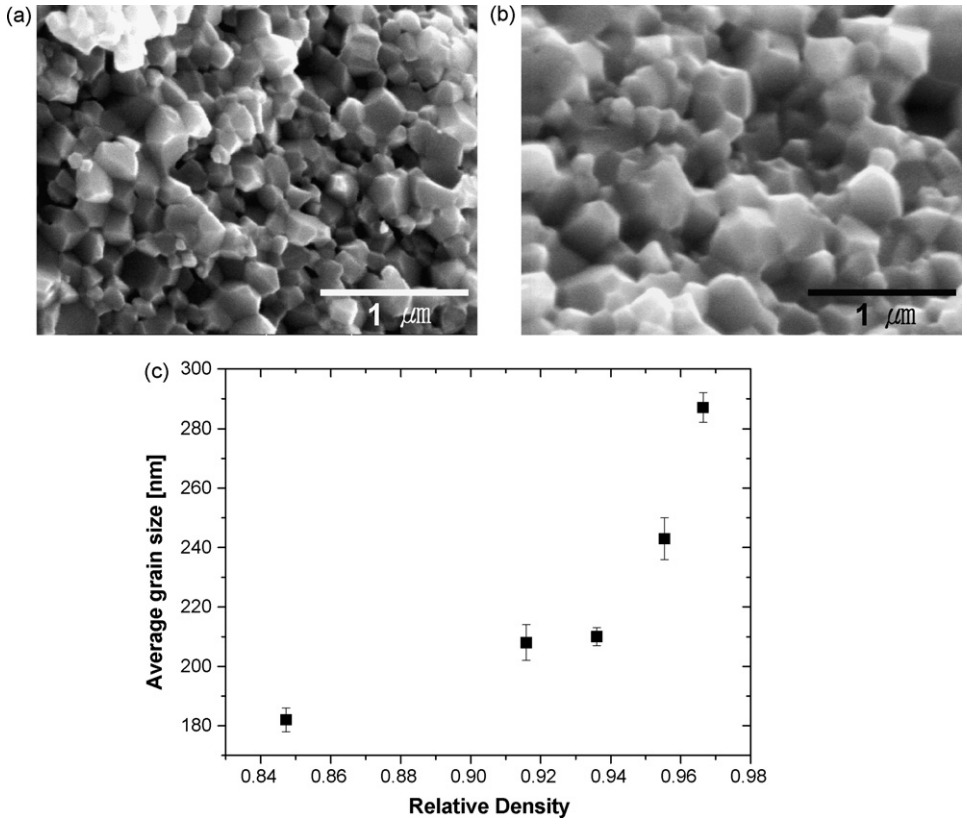

Fig. 5. SEM images of freely sintered GDC at the density of (a) 84.7 and (b) 96.7%. Sintering trajectory of freely sintered pellets at 1100 °C (c).

where E_p^0 is a scaling factor, $E_p^1(\rho)$ and $E_p^2(d)$ are the functions independent to grain size and density, respectively. This general expression can also be adapted to bulk and shear viscosities as well as to the sintering stress.[14,15] According to theoretical descriptions,[7,11,16,32,33] the viscosity increases with an increased relative load bearing area ϕ, which is the ratio of the load bearing area over the cross-sectional area of the specimen. This can be expressed as a function of porosity of density $E_p^1(\rho)$. At lower densities, owing to the small value of ϕ, uniaxial viscosity remains low and shows a moderate increase up to 90% of the relative density. If densification proceeds, grain coarsening also affects the viscosity of the sintering material. The function $E_p^2(d)$ is proportional to the cube of the grain size normalized by the initial grain size for the case of grain boundary diffusion.[14,15,31,32]

Various models have been proposed for the viscosity of porous powder compact as a function of relative density and grain size. To compare the measured viscosity with those estimated by different models, the sintering trajectory during free sintering at 1100 °C was measured. Fig. 5(a) and (b) shows the fracture surfaces of the freely sintered specimens with 84.7 and 96.7% of relative density. Fig. 5(c) is a plot of grain size and relative density of sintered specimens. Densification as well as grain growth occurs; however, the grain growth rate increases as the relative density increases. Nevertheless the grain size remains less than 0.3 μm at 97% of relative density. A similar result was also observed by Jud et al.[34] for pellets made of the same GDC powder.

Fig. 6 plots the measured uniaxial viscosity at 1100 °C normalized by the value measured at 85% of density as well as those calculated using the models of Rahaman et al.,[32] Hsueh et al.,[13] Riedel et al.,[15] Venkatachari and Raj,[33] and Scherer.[7] All these models include a function of grain size, except Scherer's one, which is used to emphasize the effect of grain growth. The equations used for the viscosity calculation of each models are listed in Appendix A. Rahaman, Hsueh and Riedel's models show good agreement with the measured data (the difference remains less than 20% over the whole density range), whereas Venkatachari and Scherer's models underestimate the viscosity.

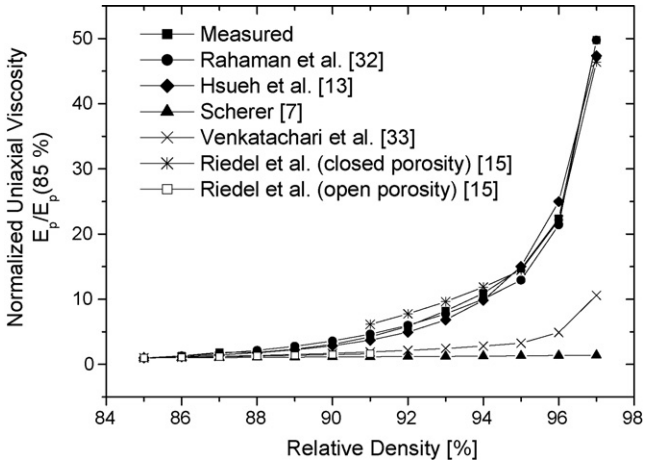

Fig. 6. Comparison between measured uniaxial viscosity normalized by density and theoretical predictions.

In Fig. 6, Rahaman's model appears to best fit the measured data. Rahaman's model[32] relies on Beere's geometrical relationship for a definite grain/pore configuration[35] and Coble's creep formalism.[36] The pore geometry was based on a corner unit having tetragonal symmetry during the intermediate stage of sintering. The fraction of load bearing area was defined as follows:

$$\phi = \exp(-aP) \tag{4}$$

where a is a constant determined by the apparent dihedral angle ψ and $P = 1 - \rho$ is the porosity. As a fitting parameter, a was found to be 10.5 in this study. Rahaman and De Jonghe[37] reported that a was equal to 5 for ZnO ($\psi = 120°$) whereas it was 2 for CdO ($\psi = 125°$).[32] Here, GDC has an apparent dihedral angle of $116 \pm 4°$ measured by TEM. A smaller value than that measured on CdO and ZnO leads to a higher value of a. In Beere's geometrical model, a is inversely proportional to the dihedral angle. According to the present result, the dependence of a on the dihedral angle seems to be more important than predicted by Beere's model. A possible explanation is that the number of pores per grain does not remain constant for the whole range of density (here, samples were sintered until pore closure, which can introduce major changes in the microstructure).

Hsueh et al.[13] did not define the fraction of the load bearing area, but predicted an increase of uniaxial viscosity with grain growth for high density range. Even if grain size was not explicitly taken into account as a variable, their prediction for uniaxial viscosity at the late stage of sintering is in good agreement with the present experimental data. They suggested the following equation for the shear viscosity:

$$G_p = G_p^0 \rho^p (1 - \rho)^{-\lambda} \tag{5}$$

where G_p^0 is a scaling factor which depends on temperature, initial grain size and initial density, p and λ are fitting parameters. The second term on the right-hand side gives the dependence of the shear viscosity on density at constant grain size and the third term indirectly takes the grain growth into account.[9] Values of 0.5 and 1.67 for p and λ were evaluated for Coble and Kingery's data.[36] In this study, p and λ were equal to 0.4 and 1.35, respectively.

Riedel et al.[14,15] adopted grain boundary diffusion as a dominant mass transport mechanism to build two distinctive sets of constitutive equations for the intermediate and late stages of sintering. Several elementary cell configurations were employed to compute equilibrium surface areas. The relevant coefficients for the parabolic fit functions were then determined numerically. Here, the pore coordination number was assumed to be 8 for the intermediate stage model. They also developed a special geometry for the case of closed porosity. The relationship between the shear and bulk viscosities is defined in the Appendix A. Although the structure of a virtual material is reproduced (under the assumption of spherical and monosized particles), this model does not give a continuity in viscosity (and sintering stress) when the type of the porosity changes from open to closed. This problem can be circumvented, if the geometrical transition occurs over a range of the densities.[26]

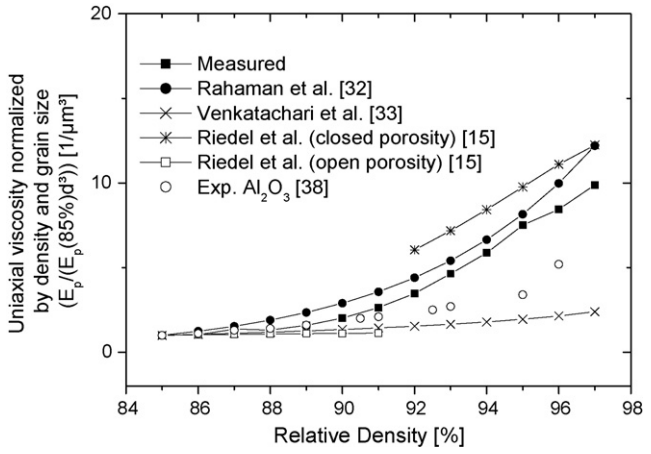

Fig. 7. Comparison between measured and modelled uniaxial viscosity normalized by density and grain size.

Venkatachari and Raj[33] derived constitutive laws from a hot forging study of magnesia doped alumina. They found that Coble's creep behaviour fit their experimental data, but used a simpler form for the load bearing area than Rahaman et al., ϕ being defined as the inverse of the relative density. This simple function of density seems to be cause of the poor agreement between the calculated and experimental curves.

To predict the sintering behaviour of sol–gel glasses, Scherer adopted a cubic cell. In that case, there was no consideration of grain growth as it was developed for viscous materials.[7,8] The considerable discrepancy between the calculated and experiment value, in particular for densities above 90%, must be due to the ignorance of grain growth.

All theoretical frameworks presented here, except Hsueh's and Scherer's, use explicitly the same function of grain size $E_p^2(d) = d^3$. In order to highlight the differences among the tested models, the normalized viscosity presented in Fig. 6 was divided by the cube of the normalized grain size to take the grain growth into account. Although the grain growth was not considerable, less than doubled (Fig. 5(c)), the difference in viscosity between the analysis with (Fig. 7) and without (Fig. 6) grain growth consideration is more than five times. This highlights the remarkable contribution of grain coarsening on the viscosity. Fig. 7 also shows more distinctly the difference between the measured values and the calculated values from different models. The viscosity calculated using Riedel's model is underestimated for the relative density range between 89 and 91% while it is overestimated for the range over 91%. The difference between measured and the calculated using Venkatachari's model increases with an increased relative density and is considerable at final stage sintering. Rahaman's prediction, however, lies very close to the measured curve, showing that the present GDC pellets behave similarly to the CdO material used in their study. For comparison, the experimental data of alumina pressure-filtrated specimens[38] is also plotted. It shows a lower dependence of the normalized viscosity on the relative density, meaning that the load bearing area is affected by the powder and the manufacturing process.

The analysis and discussion so far assumed that the relative density and the average grain size were the microstructural parameters affecting the viscoelastic properties. However, the equilibrium dihedral angle can be another important microstructural parameter, as Riedel et al. suggested.[14,15] The neck radius can also affect the viscosity were significantly than the relative density, as Bouvard and Meister noted.[16] To predict the change in viscosity in terms of overall (density and grain size) and local (dihedral angle and neck radius) microstructure, the development of a more sophisticated model should be needed.

4. Conclusion

Discontinuous sinter forging has been performed with a high-resolution laser-assisted sinter forging apparatus on nanocrystalline gadolinium-doped ceria. The measured axial strain rates showed good linearity with respect to the applied stress and allowed us to determine the uniaxial viscosity at 1100 °C. The effects of the relative density and grain coarsening were taken into account. A comparison with available models showed that the prediction by Rahaman best fits the experimental data.

Acknowledgements

A part of this work was supported by The Core Technology Development Program for Fuel Cells of the Ministry of Commerce, Industry and Energy in Korea (Grant No. 10022724-2005-12). Mr. J.-B. Ollagnier is acknowledged for helpful discussion.

Appendix A. Equations used for the calculations of uniaxial viscosity

A.1. Rahaman et al.[32]

$$G_p = A \times d^3 \times \rho \times \exp[-2a(1-\rho)]$$
$$K_p = A \times d^3 \times \rho \times \exp[-a(1-\rho)]$$
$$E_p = \frac{9K_pG_p}{3K_p + G_p} \quad \text{and} \quad E_p^1(\rho) = \rho\frac{\exp[-3a(1-\rho)]}{3\exp[-a(1-\rho)] + \exp[-2a(1-\rho)]}$$

A.2. Hsueh et al.[13]

$$G_p = G_p^0 \times \rho^p(1-\rho)^{-\lambda}$$
$$K_p = -K_p^0\frac{\rho \times \lambda(1-\rho)^{\lambda}}{(1-\rho)^{1+\lambda}}$$
$$E_p = \frac{9K_pG_p}{3K_p+G_p} = 9G_p^0 \times K_p^0 \times \rho \times \lambda\frac{(1-\rho)^{-\lambda}(1-\rho_o)^{\lambda}}{G_p^0(1-\rho) + 3K_p^0 \times \rho^{1-p} \times \lambda(1-\rho_o)^{\lambda}}$$

A.3. Riedel et al.[15]

For the intermediate stage of sintering:

$$K_p^1(\rho) = (\alpha_o + \alpha_1\psi + \alpha_2\psi^2) + (\beta_o + \beta_1\psi + \beta_2\psi^2)(1-\rho) + (\gamma_o + \gamma_1\psi + \gamma_2\psi^2)(1-\rho)^2$$

where ψ is the equilibrium dihedral angle.

For the final stage of sintering:

$$K_p^1(\rho) = \frac{1}{\rho}\left(-2\ln(\xi\omega) - \frac{33}{64} + \xi\omega - \frac{(\xi\omega)^2}{16}\right)$$

where ξ is a geometry factor,

$$\varpi(\rho, \psi) = 6^{1/3}\left(\frac{1-\rho}{4h(\psi)}\right) \quad \text{and}$$

$$h(\psi) = \frac{(1+\cos(\psi/2))^{-1} - (1/2)\cos(\psi/2)}{\sin(\psi/2)}$$

$G_p^1(\rho)$ is calculated from:

$$\frac{G_p^1}{K_p^1}(\rho) = [0.27 + 2(\rho - 0.62)^2]\left[1 - \left(\frac{0.4}{1.4-\rho}\right)^{12}\right]$$

Finally, $E_p^1(\rho) = \frac{K_p^1 G_p^1}{3K_p^1 + G_p^1}$

A.4. Venkatachari and Raj[33]

$$G_p = G_p^0 \times d^3 \times \rho$$

$$K_p = K_p^0 \times d^3 \times \frac{1}{\rho}[\ln(1-\rho) + 0.5\rho(\rho+2)]$$

$$E_p^1(\rho) = \rho\frac{\ln(1-\rho) + 0.5\rho(\rho+2)}{(3K_p^0/\rho)[\ln(1-\rho) + 0.5\rho(\rho+2)] - G_p^0 \times \rho}$$

A.5. Scherer[7,8]

$$E_p = 3A\left(\frac{\rho}{3-2\rho}\right)$$

References

1. Minh, M. Q. and Takahashi, T., *Science and Technology of Ceramic Fuel Cells*. Elsevier, Amsterdam, 1995.
2. Singh, P. and Minh, N. Q., Solid oxide fuel cells: technology status. *Int. J. Appl. Ceram. Technol.*, 2004, **1**, 5–15.
3. Inaba, H. and Tagawa, H., Ceria-based solid electrolytes. *Solid State Ionics*, 1996, **83**, 1–16.
4. Goodenough, J. B., Oxide-ion electrolytes. *Annu. Rev. Mater. Res.*, 2003, **33**, 91–128.
5. Yokokawa, H., Sakai, N., Horita, T. and Yamaji, K., Recent developments in solid oxide fuel cell materials. *Fuel Cells*, 2001, **1**, 117–131.
6. Cai, Z., Lan, T. N., Wang, S. and Dokiya, M., Supported Zr(Sc)O-2 SOFCs for reduced temperature prepared by slurry coating and co-firing. *Solid State Ionics*, 2002, **152**, 583–590.
7. Scherer, G. W., Sintering Inhomogeneous glasses: application to optical waveguides. *J. Non-Cryst. Solids*, 1979, **34**, 239–256.
8. Scherer, G. W., Viscous Sintering under a uniaxial load. *J. Am. Ceram. Soc.*, 1986, **69**, C206–C207.
9. Bordia, R. K. and Scherer, G. W., On constrained sintering. II. Comparison of constitutive models. *Acta Mater.*, 1988, **36**, 2399–2409.
10. McMeeking, R. M. and Kuhn, L. T., A diffusional creep law for powder compacts. *Acta Metall. Mater.*, 1992, **40**, 961–969.
11. Du, Z. Z. and Cocks, A. C. F., Constitutive models for the sintering of ceramic components. 1. Material models. *Acta Mater.*, 1992, **40**, 1969–1979.
12. Cocks, A. C. F., The structure of constitutive laws for the sintering of fine-grained materials. *Acta Metall. Mater.*, 1994, **42**, 2191–2210.
13. Hsueh, C. H., Evans, A. G., Cannon, R. M. and Brook, R. J., Viscoelastic stresses and sintering damage in heterogeneous powder compacts. *Acta Metall.*, 1986, **34**, 927–936.
14. Svoboda, J., Riedel, H. and Zipse, H., Equilibrium pore surfaces, sintering stresses and constitutive-equations for the intermediate and late stages of sintering. 1. Computation of equilibrium surfaces. *Acta Metall. Mater.*, 1994, **42**, 435–443.
15. Riedel, H., Zipse, H. and Svoboda, J., Equilibrium pore surfaces, sintering stresses and constitutive-equations for the intermediate and late stages of sintering. 2. Diffusional densification and creep. *Acta Metall. Mater.*, 1994, **42**, 445–452.
16. Bouvard, D. and Meister, T., Modelling bulk viscosity of powder aggregate during sintering. *Model. Simul. Mater. Sci. Eng.*, 2000, **8**, 377–388.
17. Skorokhod, V. V., *Rheological Basis of the Theory of Sintering*. Naukova Dumka, Kiev, 1972.
18. Boutz, M. M. R., Winnubst, L. and Burggraaf, A. J., Low-temperature sinter forging of nanostructured Y-TZP and YCe-TZP. *J. Am. Ceram. Soc.*, 1995, **78**, 121–128.
19. Cai, P. Z., Messing, G. L. and Green, D. J., Determination of the mechanical response of sintering compacts by cyclic loading dilatometry. *J. Am. Ceram. Soc.*, 1997, **80**, 445–452.
20. Bang, J., Lu, G. Q. and Calata, J. N., Determination of shear viscosity of borosilicate glass plus silica powder compacts by an optical system. *J. Mater. Res.*, 1999, **14**, 1062–1068.
21. Gillia, O., Josserond, C. and Bouvard, D., Viscosity of WC-Co compacts during sintering. *Acta Mater.*, 2001, **49**, 1413–1420.
22. Lee, S. H., Messing, G. L. and Green, D. J., Bending creep test to measure the viscosity of porous materials during sintering. *J. Am. Ceram. Soc.*, 2003, **86**, 877–882.
23. Zuo, R., Aulbach, E., Bordia, R. K. and Rödel, J., Critical evaluation of hot forging experiments: case study in alumina. *J. Am. Ceram. Soc.*, 2003, **86**, 1099–1105.
24. Zuo, R., Aulbach, E. and Rödel, J., Experimental determination of sintering stresses and sintering viscosities. *Acta Mater.*, 2003, **51**, 4563–4574.
25. Aulbach, E., Zuo, R. and Rödel, J., Laser-assisted high-resolution loading dilatometer and applications. *Exp. Mech.*, 2004, **44**, 71–75.
26. Kanters, J., Eisele, U. and Rödel, J., Cosintering simulation and experimentation: case study of nanocrystalline zirconia. *J. Am. Ceram. Soc.*, 2001, **84**, 2757.
27. Lee, S. H., Messing, G. L. and Green, D. J., Warpage evolution of screen printed multilayer ceramics during co-firing. *Key Eng. Mater.*, 2004, **264–268**, 321–328.
28. Ravi, D. and Green, D. J., Sintering stresses and distortion produced by density differences in bi-layer structures. *J. Eur. Ceram. Soc.*, 2006, **26**, 17–25.
29. Horovistiz, A. L., Frade, J. R. and Hein, L. R. O., Comparison of fracture surface and plane section analysis for ceramic grain size characterization. *J. Eur. Ceram. Soc.*, 2004, **24**, 619–626.
30. Kleinlogel, C. and Gauckler, L. J., Sintering and properties of nanosized ceria solid solutions. *Solid State Ionics*, 2000, **135**, 567–573.
31. Li, J.-G., Ikegami, T. and Mori, T., Low temperature processing of dense samarium-doped CeO_2 ceramics: sintering and grain growth behaviors. *Acta Mater.*, 2004, **52**, 2221–2228.
32. Rahaman, M. N., DeJonghe, L. C. and Brook, R. J., Effect of shear-stress on sintering. *J. Am. Ceram. Soc.*, 1986, **69**, 53–58.
33. Venkatachari, K. R. and Raj, R., Shear deformation and densification of powder compacts. *J. Am. Ceram. Soc.*, 1986, **69**, 499–506.
34. Jud, E., Huwiler, C. B. and Gauckler, L. J., Sintering analysis of undoped and cobalt oxide doped ceria solid solutions. *J. Am. Ceram. Soc.*, 2005, **88**, 3013–3019.

35. Beere, W., Unifying theory of stability of penetrating liquid-phases and sintering pores. *Acta Metall.*, 1975, **23**, 131–138.
36. Coble, R. L. and Kingery, W. D., Effect of porosity on physical properties of sintered alumina. *J. Am. Ceram. Soc.*, 1956, **39**, 377–385.
37. Rahaman, M. N. and De Jonghe, L. C., Creep-sintering of zinc oxide. *J. Mater. Sci.*, 1987, **22**, 4326–4330.
38. Guillon, O., Bordia, R. and Rödel, J., Effect of green state processing on the sintering stress and viscosity of alumina compacts. *J. Am. Ceram. Soc.*, in press.